Lab on a Chip

COMMUNICATION

View Article Online
View Journal | View Issue

Cite this: *Lab Chip*, 2025, **25**, 4577

Received 16th June 2025,
Accepted 25th July 2025

DOI: 10.1039/d5lc00590f

rsc.li/loc

Design and characterization of a self-powered microneedle microfluidic system for interstitial fluid sampling

Christopher T. Sharkey,†[a] Angélica F. Aroche,†[b] Isabella G. Agusta,†[b] Hannah Nissan,[a] Tamoghna Saha,[c] Sneha Mukherjee,[c] Jack S. Twiddy,[b] Michael D. Dickey,[c] Orlin Velev[c] and Michael A. Daniele *[ab]

Dermal interstitial fluid (ISF) is a promising source of biomarkers for point-of-care (PoC) diagnostics, yet noninvasive and reliable extraction remains a significant challenge. In this study, we present a fully passive microneedle (MN) platform that integrates hydrogel-forming MNs, a hydrogel-based osmotic pump, and paper microfluidics to enable zero-power ISF extraction and analyte transport from skin models. The system's performance was evaluated using paper microfluidic designs optimized for both bulk fluid uptake and lateral flow-based detection. Osmotic pumping with glycerol and glucose showed comparable extraction efficiencies. Cortisol, a representative stress biomarker, was successfully recovered following 15-minute, 45-minute, and 24-hour sampling durations, demonstrating the platform's suitability for both short-term and extended ISF monitoring. These results highlight the potential of this integrated MN system as a simple, cost-effective, and minimally invasive solution for passive ISF sampling and subsequent biochemical analysis.

Introduction

Wearable and point-of-care (PoC) diagnostic systems have shown exciting potential for decentralized biomarker monitoring in research settings, but very few have translated into real-world utilization for clinical decision making and lifestyle management; continuous glucose monitors (CGMs) remain one of the only widespread successes. Recent research and commercialization efforts for sweat-based diagnostic systems have shown some promise.[1–6] However, sweat is primarily composed of small, metabolically relevant molecules such as glucose, lactate, and electrolytes, containing only trace amounts of proteins and high molecular weight biomarkers.[7,8] This significantly limits the range of molecules, and consequently diseases/physiological states, which may be assessed using sweat. Furthermore, because sweat must pass through glandular pathways and skin layers, there is a greater temporal delay between blood (the gold standard diagnostic biofluid) biomarker concentration changes and their appearance in sweat, which restricts the timeliness and actionability of sweat-based diagnostics in some applications.[9,10]

For PoC health monitoring, interstitial fluid (ISF) is a more attractive diagnostic medium than sweat. This extracellular fluid, located in the spaces between cells, serves as an excellent proxy for blood biomarkers because it acts as the primary transport medium between capillaries and cells, reflecting changes in blood molecules with minimal temporal delay. The clinical validity of ISF as an indicator for blood biomarker concentrations is evident by the commercial success of CGMs, which measure glucose concentrations in ISF. Additionally, ISF demonstrates near homogeneity with blood in terms of protein diversity, indicating that a myriad of biomarkers can be monitored in ISF. Prior studies have shown that 90–99% of blood proteins are present in ISF.[11,12] It has also been demonstrated by proteomic analysis that some proteins present in ISF are not found in blood, indicating that this biofluid offers unique diagnostic opportunities.[13]

While ISF is present throughout the body, its superficial presence in the dermis and epidermis makes it easily accessible through the skin. Of the three major anatomical skin layers (epidermis, dermis, and hypodermis), ISF is most abundant in the dermis due to its extensive vascularization and limited connective tissue. Prior studies have indicated that the dermis is comprised of approximately 50–70% ISF by volume.[14,15] The primary physical barriers to dermal ISF extraction are the stratum corneum and the viable epidermis. These two layers represent a combined thickness of 50–200

[a] *Department of Electrical & Computer Engineering, North Carolina State University, 890 Oval Dr, Raleigh, NC 27695, USA. E-mail: mdaniel6@ncsu.edu*
[b] *Joint Department of Biomedical Engineering, North Carolina State University and University of North Carolina, Chapel Hill, 1840 Entrepreneur Dr, Raleigh, NC 27695, USA*
[c] *Department of Chemical & Biomolecular Engineering, North Carolina State University, Raleigh, NC 2769, USA*
† These authors contributed equally to this work and share first authorship.

μm, indicating that a penetration depth greater than 200 μm is sufficient to access dermal ISF.[16]

Despite the attractiveness of ISF for wearable and PoC health monitoring, it remains underutilized due to the lack of minimally invasive, painless, and wearable methods of accessing and/or extracting ISF for analysis. Conventional techniques (*e.g.*, suction blistering, microdialysis and open flow microperfusion) are painful, time consuming and invasive.[17–19] None of these ISF extraction methods are well-suited for frequent PoC applications, as they pose substantial translational challenges in terms of patient compliance, comfort, and usability. Moreover, the equilibration dynamics and temporal kinetics of analyte distribution between blood and ISF remain incompletely understood,[14,20,21] presenting an additional barrier to adoption of ISF-based diagnostic systems. The invasive and expensive nature of conventional ISF extraction techniques presents a barrier to eliminating this knowledge gap and realizing general ISF diagnostics, necessitating the development of alternative tools for ISF acquisition.

Since early demonstrations as diagnostic tools, microneedles (MNs) have emerged as a compelling means of accessing dermal ISF in a minimally invasive manner.[22–24] Typically measuring 300–1000 μm in length, MNs can penetrate the stratum corneum and viable epidermis while avoiding deeper dermal regions rich in nociceptors and blood vessels.[14] This permits access to ISF with minimal pain, negligible interference from blood, and minimal risk of tissue damage or scarring. MNs can be produced using scalable microfabrication or micromolding methods[25,26] and can be combined with flexible substrates to support wearable form factors.[27,28]

A wide variety of materials, including metals (*e.g.*, titanium, stainless steel), ceramics (*e.g.*, silicon, alumina), and polymers (*e.g.*, polycarbonate, polyethylene glycol diacrylate, polyvinyl acetate, and methacrylated hyaluronic acid), have been employed to tailor the mechanical strength, biocompatibility, and ease of integration of MN systems.[29] Diagnostic MN systems may extract ISF for downstream, *ex vivo* biosensing or function as *in situ* biosensors within the dermis, with conductive microneedle materials enabling electrochemical sensing.[30–33] Among polymeric MNs, hydrogel-forming MNs represent a distinct class that swell upon insertion, passively absorbing ISF without degrading. Hydrogel-forming MNs are attractive for PoC applications due to their biocompatibility, ease of fabrication and low cost. However, they may extract smaller fluid volumes and have reduced mechanical robustness in comparison to metallic or ceramic MNs, limiting their utility for prolonged extraction.[34]

Many prior works have demonstrated that a variety of MN systems may be used for ISF-based diagnostics[22–24,30–33,35] but translating these systems into practical diagnostic platforms remains challenging.[14] For viability in PoC and wearable applications where resources may be constrained, a MN system must consistently access or extract sufficient ISF (1–20 μL) without external power, operate under varying environmental conditions, and remain simple, self-administrable and cost effective. Recent efforts have addressed these needs by integrating MNs with microfluidic platforms to improve sample handling and compatibility with *ex vivo* biosensing, particularly for sensing strategies that would be impractical or unsafe *in situ*. Paper and polymer microfluidics have been especially attractive due to their low cost, ease of fabrication, and compatibility with PoC formats.[36,37] However, many of these integrated systems depend on active fluid extraction mechanisms or multilayer microfluidic architectures, which can hinder scalability and limit their suitability for translational applications like decentralized diagnostic testing.

Here, we present a wearable MN-based system that integrates hydrogel-forming MNs, paper microfluidics, and an osmotic pressure-generating hydrogel to enable zero-power extraction and storage of ISF for diagnostic applications (Fig. 1a–c(ii)). The MNs are fabricated from methacrylated hyaluronic acid (MeHA), while glycerol-loaded polyacrylamide hydrogels are used as osmotic pumps to generate passive negative pressure for ISF extraction. Analytical filter paper was cut into a microfluidic channel that facilitates ISF transport *via* capillary action, preservation of extracted biomarkers for sample storage, and compatibility with integration with *in situ* biosensors and assays for real-time diagnostics. We characterized fluid and analyte extraction from skin models across multiple osmotic pump and paper microfluidic configurations. Functionality as a diagnostic tool was demonstrated by recovery of cortisol from synthetic skin models. This steroid hormone plays a critical role in metabolism, immune activity, and stress responses, and is rapidly secreted by the adrenal gland in response to stressful situations.[38,39] Timely quantification of cortisol may enable interventions to eliminate stressors and improve health outcomes. Quantitative validation using ELISA confirmed accurate biomarker recovery within paper microfluidics over both short (15–45 min) and extended (24 h) periods of system application, supporting the system's potential for passive, PoC health monitoring.

Materials & methods

The following materials were procured from Sigma-Aldrich and used as received, unless stated otherwise: sodium hyaluronic acid (200–400 kDa, Bloomage Biotechnology Corp); methacrylic anhydride; *N*,*N*-dimethylformamide; sodium hydroxide; sodium chloride; dialysis membrane (spectra/Por 4, 12–14 kDa MWCO); 2-hydroxy-4′-(2-hydroxyethoxy)-2-methylpropiophenone; yellow fluorescent dye (Tracerline TP39000601); Parafilm® (ULine); agarose; synthetic skin (SynDaver, 2 N skin toughness, Caucasian); Sylgard 184 elastomer (Dow Corning); PBS tablets (Fisher Bioreagents); cortisol ELISA kit (Arbor Assays, K003-H); cortisol solution (1.0 mg mL^{-1} in methanol); acrylamide, *N*,*N*′-methylenebisacrylamide; glycerol; cellulose

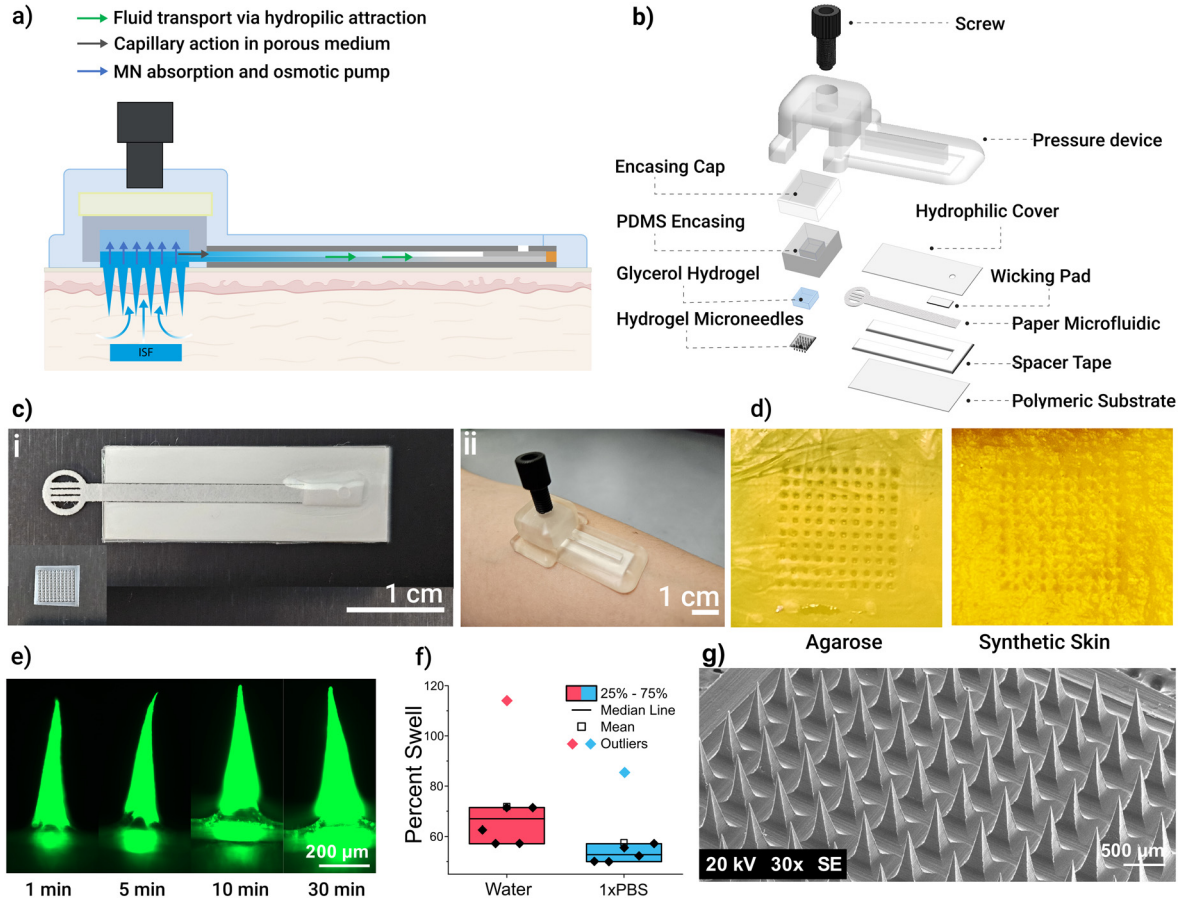

Fig. 1 Extraction system overview and preliminary assessment of fluid uptake and skin model penetration. a) Schematic of extraction system applied to human skin, displaying the different mechanisms of fluid transport within the device. b) Exploded view of the extraction system, with each component of the system labelled. c) i) Paper microfluidic and MN patch. ii) Full extraction system applied to human forearm. d) Photographs of skin models after microneedle application and removal. e) Microneedle swelling over time in response to uptake of fluorescent dye. f) Quantified microneedle swelling in response to uptake of DI water and 1× PBS (n = 6). g) Scanning electron micrograph of a single microneedle patch.

chromatography paper (Whatman® grade 1); medical adhesive tape (1577, 3M™); transport film and spacer tape (Microfluidic Diagnostic Tape 9984 and 9972A, 3M™); polymer substrate (laminating pouch, non-treated side, 3 mil; Office Depot); conjugate pad (8950 glass fiber, Ahlstrom); wicking pad (grade 222, Ahlstrom).

Microneedle fabrication

MNs were fabricated from MeHA, synthesized according to the method reported by Chang *et al.*[40] Briefly, 5 g of hyaluronic acid (200–400 kDa) was mixed with 250 mL of sterile deionized water and stirred at 4 °C for 12 h. After full dissolution, 66.6 mL of *N*,*N*-dimethylformamide and 2.38 mL of methacrylic anhydride were added. The pH was adjusted to 8–9 with 5 M NaOH and maintained for 24 h to allow for methacrylation. 12.35 g of NaCl was added at room temperature to terminate the reaction. The solution was then dialyzed against DI water at 40 °C for 5 days, frozen at −80 °C and lyophilized. MeHA was stored at 4 °C until use (Fig. S1a). A solution of 4 wt% MeHA and 0.2 wt% photoinitiator (2-hydroxy-4′-(2-hydroxyethoxy)-2-methylpropiophenone) was drop cast into PDMS molds (10 × 10 MN array, 800 µm MN height, pyramidal geometry). The filled molds were centrifuged at 3800 × g for 4 min, dried at room temperature for approximately 24 h, and removed from the molds. The MN arrays were then UV crosslinked at 30 mW cm^{-2} for 5 min (Fig. S1b).

Osmotic pump fabrication

Polyacrylamide hydrogels were prepared for osmotic pressure generation by saturating them with glycerol as the osmogen, following the method described by Saha *et al.*[41,42] The hydrogels were made from 22 wt% acrylamide monomer, 0.48 wt% *N*,*N*′-methylenebisacrylamide, and 0.15 wt% 2-hydroxy-4′-(2-hydroxyethoxy)-2-methylpropiophenone. The solution was UV cured at 100 mW cm^{-2} for 10 min. Crosslinked hydrogels were then sectioned into 5 mm^2, 2.5 mm thick pieces and stored in 12 M glycerol for at least 24 h. As an alternative osmogen, glucose was evaluated by saturating cured polyacrylamide hydrogels in 4 M glucose

rather than glycerol. Prior to use, osmotic pressure-generating hydrogels were blotted dry with a lint-free wipe to remove excess fluid.

Paper microfluidic fabrication

The paper fluidics consisted of a primary paper channel (Whatman® grade 1 chromatography paper), an absorbent pad at the terminal end, hydrophilic transport film on top, a polymer substrate on the bottom, and an intermediate adhesive spacer tape to prevent deformation of the paper channel. A schematic of the device is provided in Fig. 1b and c(i). All components were designed in SolidWorks 2023. The primary paper channel was cut to shape using a laser cutter (GlowForge™). After cutting, the paper fluidics were soaked in water for 20 min and then dried at 50 °C for approximately 1 h to remove residual contaminants from the laser cutting process. Hydrophilic transport film and spacer tape were cut using a programmable cutter (Silhouette Cameo). The paper fluidic device was assembled by placing the polymer substrate in contact with the spacer tape, followed by the paper channel, absorbent pad, and transport film. A small ventilation hole was included in the top film to facilitate air displacement during fluid absorption. Light mechanical pressure was used to seal the paper microfluidic components together (Fig. S2a). An alternative paper microfluidic design with an integrated conjugate pad was tested to assess feasibility of the MN extraction system for wearable lateral flow assay (LFA) diagnostics. In this configuration, conjugate pads bridged the paper microfluidics. The conjugate pad was soaked in 1× PBS containing 5 w/v% sucrose, 1 w/v% BSA and 0.5 v/v% Tween-20 for 15 min, then dried at 37 °C for 1 hour to facilitate reagent release. 1.5 μL of FD&C green #3 dye (a proxy LFA capture reagent) was then drop cast onto the conjugate pads and redried at 37 °C for one hour (Fig. S2b).

Auxiliary components

To retain the osmotic pump and enable application of mechanical force without significant hydrogel deformation, the osmotic pumps were placed within a PDMS casing, secured by a rigid polymer cap. An external pressure device was used to apply a consistent downward force across the assembled system, improving component contact and ensuring sufficient force during device use (Fig. S3). The PDMS casing was produced using standard molding techniques. A negative mold was designed in SolidWorks 2023 and printed on a CADWorks3D Profluidics 285D stereolithography 3D printer using Clear Microfluidic Resin with a layer height setting of 50 μm. Printed molds were rinsed with isopropyl alcohol, UV cured and coated with approximately 2 μm of parylene C to facilitate PDMS removal. Sylgard 184 PDMS was mixed at a 10 : 1 base-to-curing agent ratio, degassed in a vacuum chamber, cast into the mold, degassed again, and cured at 60 °C for 2 h before removing from the molds. A 3D printed spring-loaded applicator was used to apply MN patches to skin models consistently with sufficient force to pierce penetrable barriers without deforming the MN tips. The rigid polymer encasing cap and external pressure device were also designed in SolidWorks and fabricated using the same 3D printer and resin. The external pressure device included a threaded cavity for a 1/4–28 screw, which was manually tapped to enable adjustable force application.

Microneedle characterization & swelling assessment

Swelling of hydrogel-forming MeHA MNs was evaluated using two complementary methods. First, single MN tips were inserted into the droplet of a contact angle goniometer (Ramé-Hart) tip filled with fluid (1× PBS or deionized water) and held in place for 30 seconds. Brightfield images were captured before and after swelling (n = 6). Swelling was quantified using ImageJ by measuring the full width at half-maximum of the MN tip before and after fluid exposure. Second, swelling was visualized by immersing MNs in a 2.45 v% Tracerline® fluorescent dye solution in 1× PBS for 1, 5, 10 and 30 min. After each timepoint, individual MNs were imaged using fluorescence microscopy (EVOS FL Auto, Thermo Fisher). Representative images at each timepoint were analysed to qualitatively assess dye uptake and swelling. MNs were also imaged by scanning electron microscopy (SEM) to assess fabrication quality and applied to skin models to confirm successful insertion and penetration.

Skin models

Two alternative skin models were used to evaluate extraction performance. First, agarose skin models were prepared by heating 1.38% agarose in 1× PBS until fully dissolved, then casting into 30 mm petri dishes and cooling at 4 °C for 24 h. Gels were sectioned into 12 × 12 mm sections and immersing in analyte-containing 1× PBS for 24 h to allow for equilibration. Second, synthetic skin was cut to equivalent dimensions, rinsed thoroughly with deionized water, and immersed in analyte-loaded 1× PBS for 24 h. Prior to use, both skin model types were thoroughly blotted with a lint-free wipe to remove excess fluid and wrapped in stretched Parafilm® to simulate a penetrable barrier analogous to the stratum corneum and epidermis. The Parafilm® helped imitate the skin resistance to MN insertion. Skin models were placed in a PDMS retainer during system application. MN patches were applied to each skin model and removed to qualitatively assess penetration success.

Flow rate characterization

To characterize fluid extraction rates, skin models were prepared as previously described, with analyte equilibration occurring in 0.5 v% dye in 1× PBS. Medical adhesive tape was first applied to the skin model PDMS retainer. MNs were inserted into skin models with a spring-loaded applicator. Paper fluidics were then placed on top, followed by the osmotic pump and external pressure device, as shown in

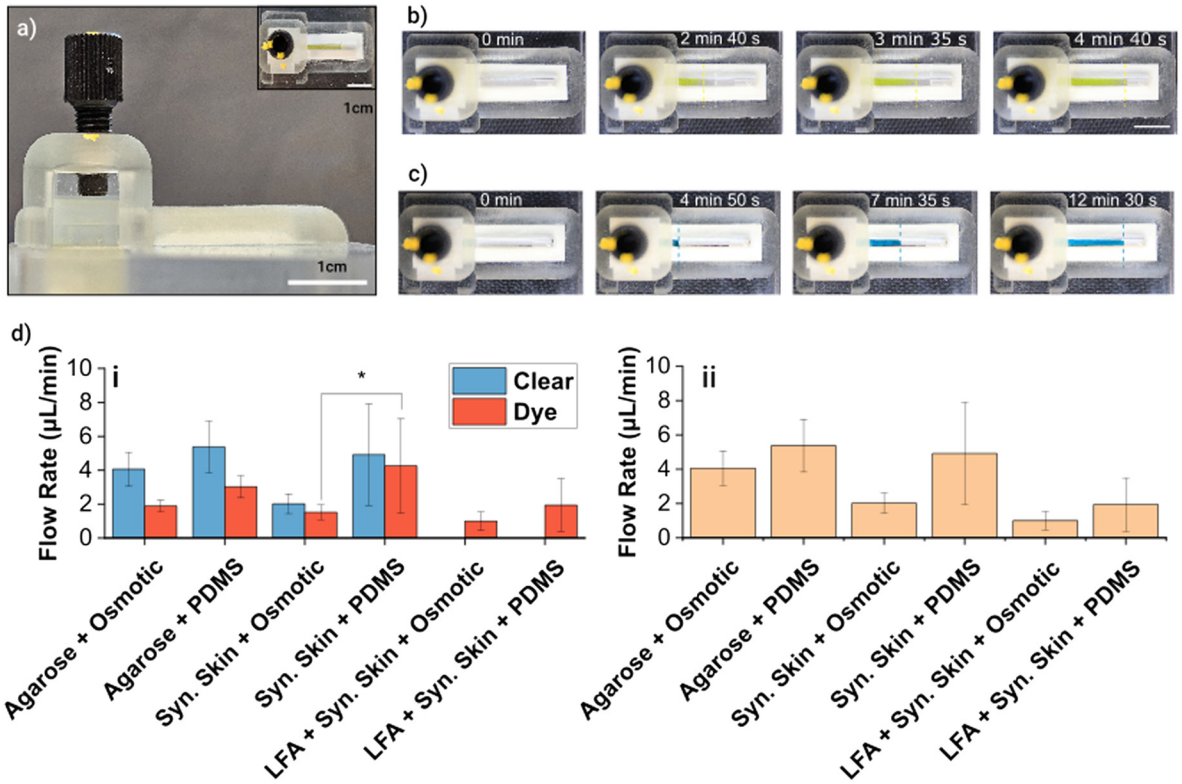

Fig. 2 Experimental setup and results for assessment of fluid and analyte extraction rates. a) Sideview and bird's eye view photographs of extraction system applied to skin models. b) Photographs of extraction system applied to dye-loaded skin model over time. c) Photographs of the extraction system with conjugate pad paper microfluidics applied to dye-free synthetic skin model over time. d) i) Measured flow rate for dye and fluid fronts across experimental configurations (n = 5). ii) Averaged dye and fluid fronts (n = 5). * = $p < 0.05$.

Fig. 2a and S4a. To further assess the utility of the osmotic pump, extraction was also tested with a PDMS cube of equivalent dimensions serving as a control in lieu of the osmotic pump. Four full rotations of the external pressure device's screw were performed to engage the extraction system. Photographs of the paper microfluidics were taken over time to track the fluid and dye front (Fig. S6). To evaluate potential integration with on-body LFAs, the alternative paper microfluidics incorporating a conjugate pad were tested (Fig. S4b). In this configuration, dye was loaded into the conjugate pad rather than the skin model. The assembled device was then applied to dye-free skin models with and without the osmotic pump, and photography was used to assess dye release and fluid flow through the conjugate pad system. To measure force applied during application, a force sensitive resistor (FSR) was inserted between the applied MN patch and osmotic pump or PDMS control. The FSR was inserted into a custom sensing circuit and voltage was logged using an Analog Discovery 2.

Cortisol extraction

Skin models for cortisol extraction were prepared as previously described, with equilibration being performed in 1× PBS containing cortisol at concentrations of 0, 12, 48, or 96 ng mL^{-1} and 0.05 v% methanol to maintain cortisol solubility. These concentrations were selected to span the range of physiologically relevant cortisol concentrations in human ISF.[43] Cortisol recovery was first assessed using a MN extraction system without integrated paper microfluidics to establish a baseline (Fig. 3a(i)). These baseline extractions were performed over durations of 45 min and 24 h, respectively. Cortisol extraction from skin models was repeated with paper microfluidics integrated into the device using extraction durations of 15 min, 45 min and 24 h. To assess the effect of different osmotic pump compositions on analyte recovery, additional agarose skin models equilibrated with 96 ng mL^{-1} cortisol were tested using MN systems containing either glucose-loaded or glycerol-loaded osmotic pumps over an extraction period of 45 min. Following each extraction period, the MN system was removed. A 3 mm biopsy punch was used to excise sections of the skin model. Paper microfluidics were manually sectioned into three distinct regions to provide spatial resolution of analyte distribution along the paper channel over time (Fig. 3b). MNs, skin model biopsies, and paper microfluidic segments were each placed in individual 2 mL microcentrifuge tubes containing 100% ethanol (55 µL for MNs and paper samples; 470 µL for skin model samples). Tubes were agitated on a plate shaker at 400 RPM for 4 h. After agitation, aliquots of ethanol extract (40 µL for MN and paper samples; 25 µL for skin model

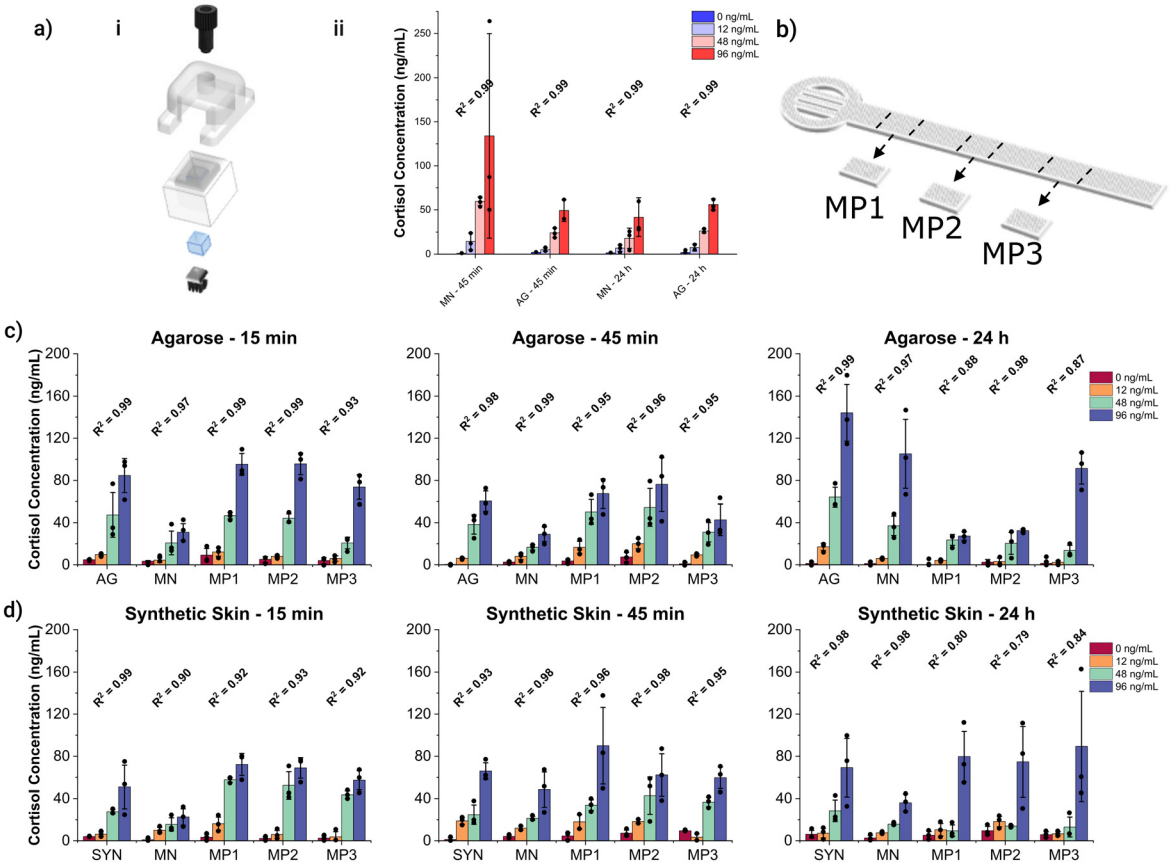

Fig. 3 Cortisol recovery from skin models using the MN extraction system. a) i) Exploded view of device configuration with no paper microfluidics for preliminary assessment of cortisol extraction. ii) Recovered cortisol from MN samples and agarose (AG) skin models after 45 min and 24 h of application (n = 3). b) Schematic of microfluidic paper (MP) sample labelling used in Fig. 3c. c) Recovered cortisol from MN samples, AG models, and MP samples after 15 min, 45 min and 24 h of application (n = 3). d) Recovered cortisol from MN samples, synthetic skin models, and MP samples after 15 min, 45 min and 24 h of application (n = 3).

samples) were transferred to fresh 2 mL microcentrifuge tubes and evaporated under vacuum for one hour. Dried samples were reconstituted in 55 μL of 1× assay buffer (Arbor Assays) and cortisol content was measured by ELISA. Final sample concentrations were calculated according to measured fluid volumes per sample type and dilution factors used during sample processing (see SI, Table S1). A summary of all MN extraction system configurations used for flow rate and cortisol extraction experiments is provided in Table S2.

Statistical analysis

All statistical analysis was performed using GraphPad Prism 8. Data are presented as mean ± standard deviation unless otherwise noted. Individual MN swelling assessments were performed with six replicates. Flow rate assessments were performed with five replicates. All other experiments were performed in triplicate. Comparisons were conducted using unpaired Student's t-test with Holm–Sidak correction for multiple comparisons. Statistical significance was defined as $p < 0.05$ (*), $p < 0.01$ (**), and $p < 0.001$ (***).

Results & discussion

While wearable systems for ISF extraction have shown promise for minimally invasive PoC diagnostics, most existing systems depend on active pumping mechanisms and involve complex and costly fabrication. This study evaluated a fully passive wearable system integrating hydrogel-forming MNs, paper microfluidics, and an osmotic pump for ISF extraction and cortisol recovery from skin models. The subcomponents of the MN extraction system and a fully assembled device are shown in Fig. 1b and c. To the authors' knowledge, this is the first demonstration of cortisol recovery from skin models using an MN extraction system. To characterize the performance of our wearable ISF extraction system, we performed a series of experiments measuring fluid uptake, analyte transport, and cortisol recovery using synthetic skin models. The system demonstrated rapid MN swelling, consistent fluid and dye transport through paper microfluidics, and accurate cortisol recovery across a physiologically relevant range. Statistically significant differences in recovered cortisol quantities across test conditions further support the system's ability to resolve

physiologically relevant variations in biomarker concentrations. These findings support the potential of this platform as a rapid, minimally invasive, zero-power PoC diagnostic platform for ISF.

Microneedle characterization & swelling assessment

SEM imaging confirmed high-quality MN fabrication (Fig. 1g), and penetration tests showed consistent insertion of MNs into skin models (Fig. 1d). Individual MeHA MNs demonstrated rapid swelling and fluid uptake upon contact with aqueous environments. Exposure to fluorescent dye in 1× PBS resulted in consistent swelling of MNs over a 30-minute duration (Fig. 1e). With 30 seconds of fluid contact, quantitative analysis of imaged MN tips showed an average MN full width at half maximum increase of 72% ± 6% for DI water and 58% ± 3% for 1× PBS (Fig. 1f). These results are consistent with prior reports of MeHA MNs demonstrating rapid swelling within seconds to minutes of exposure to aqueous media.[44,45] Our slightly lower degree of swelling resulted from increased UV crosslinking during MN fabrication, which reduces overall fluid uptake capacity.

Flow rate characterization

For all combinations of skin model (agarose or synthetic) and osmotic pump configuration (glycerol-loaded hydrogel or PDMS) using standard paper microfluidics, both fluid and dye consistently travelled the full length of the paper channel within 10 min (Fig. S6). In agarose-based skin models, fluid flow rates ranged from 4–5.5 μL min^{-1} and dye transport from 1.5–3.5 μL min^{-1} (Fig. 2b and d(i-ii)). The lower range of the reported flow rates were observed in setups with the osmotic pump, while higher flow rates correspond to the PDMS control. However, configurations utilizing the osmotic pump consistently exhibited lower standard deviations than those using the PDMS control. When synthetic skin was used, both fluid and dye transport were reduced. Flow rates ranged from 2–5 μL min^{-1} for fluid and 1.5–4.5 μL min^{-1} for dye (Fig. 2d(i-ii)). A statistically significant difference in dye transport was observed between osmotic pump and control conditions in synthetic skin models ($p < 0.05$), but not in agarose-based models. (Fig. 2d(i)). When fluid and dye flow was averaged (Fig. 2d(ii)), no statistically significant differences were found between pump configurations for either skin model. In experiments incorporating a conjugate pad configuration, dye was consistently transported through the full paper channel within 15 min (Fig. 2c and S6). Dye flow rates in this configuration were approximately 1 μL min^{-1} with the osmotic pump and 2 μL min^{-1} for the control. Flow rate assessments and cortisol recovery from skin models indicate that accurate quantification of analytes can be achieved within 15 min. Across all test conditions, fluid and dye extraction were on average higher in PDMS control configurations than those with an osmotic pump. The lower standard deviation of fluid extraction rates from osmotic pumping configurations suggests that osmotic pumping enables more predictable and uniform fluid extraction. This consistency is critical for achieving timely and accurate diagnostic measurements, highlighting the advantage of osmotic pumping for controlled ISF extraction.

To account for variability in flow rate assessments arising from differences in applied force on the model skin, forces generated by both standard weight loading and external device screw-tightening were quantified (Fig. S5a). Measurements indicated that the PDMS configuration exerted greater force on the skin models compared to the osmotic pump configuration under equivalent loading conditions (Fig. S5b and c). This discrepancy is due to the relative compressibility of polyacrylamide hydrogels *versus* PDMS, with the latter promoting mechanical fluid expulsion rather than passive extraction driven by an osmotic pressure gradient. Although the osmotic pump configuration exhibited lower flow rates *in vitro*, it is expected to offer greater utility *in vivo*, where variations in skin elasticity and surface topology can hinder mechanically assisted extraction and introduce variability. In such contexts, sustained osmotic pressure gradients may provide more consistent and physiologically compatible ISF acquisition.

Cortisol extraction

To evaluate the performance of the platform under various operating conditions, we conducted a series of experiments comparing cortisol recovery with and without integrated paper microfluidics across multiple extraction durations and cortisol concentrations. These studies aimed to assess the linearity and temporal dynamics of cortisol extraction from skin models, as well as to investigate spatial analyte distribution along the microfluidic pathway. Additionally, we examined the impact of osmogen type on system performance to inform future integration strategies. The results provide insight into the system's capacity for rapid, minimally invasive sampling and its limitations over prolonged application periods.

Cortisol extraction without integrated paper microfluidics demonstrated a strong linear relationship between the initial cortisol concentration in the skin model and the amount recovered from the MN patch after both 45 min (R^2 = 0.9969) and 24 h (R^2 = 0.99064) of extraction (Fig. 3a(ii)). Notably, MN patches recovered approximately two to threefold more cortisol at 45 min compared to 24 h, suggesting potential depletion effects over prolonged extraction periods. For 45-minute extractions, statistically significant differences between cortisol recovered from MNs and skin models were observed at concentrations of 0 ng mL^{-1} ($p < 0.05$) and 48 ng mL^{-1} ($p < 0.01$) (Fig. S8a(ii)). A higher standard deviation occurred in MNs applied to skin models loaded with 96 ng mL^{-1} for 45 min due to a single replicate with elevated recovery. Across tested skin model concentrations, many

instances of statistically significant differences in recovered cortisol from MNs were observed (Fig. S8a(i)).

When paper microfluidics were integrated into the system, a strong positive relationship was again observed between cortisol in skin models and the amount recovered from both MN patches and paper microfluidic segments following application times of 15 min and 45 min (Fig. 3c and d), as indicated by high R^2 values ($R^2 > 0.9$). Although some significant differences were observed between MNs and microfluidic paper segments, only three instances of significant differences between recovered cortisol from skin models and extraction system components were observed (48 ng mL^{-1} cortisol, 15 min, synthetic skin *vs.* microfluidic paper segment 3, $p < 0.05$; 48 ng mL^{-1} cortisol, 15 min, synthetic skin *vs.* microfluidic paper segment 1, $p < 0.001$; 0 ng mL^{-1} cortisol, 45 min, synthetic skin *vs.* microfluidic paper segment 3, $p < 0.01$) (Fig. S8b(ii)). Several instances of statistically significant differences between individual extraction system subcomponents exposed to different cortisol concentrations were observed (Fig. S8b(i)). To assess spatial variations in extraction and analyte equilibration over time, the microfluidic paper channel was segmented into three regions. After 15 min of application, many instances of statistically significant differences in cortisol recovery in distal MP segments (MP2, MP3) in comparison to skin models were observed. Similarly, after 45 min of system application, statistically significant differences in cortisol recovery between skin models and microfluidic paper segments were only observed in MP3.

After 24 h, cortisol in MN patches and skin model biopsies maintained a strong direct relationship, but recovery of cortisol from paper microfluidic segments showed diminished consistency, particularly at lower cortisol concentrations (0–48 ng mL^{-1}). Despite this, the system retained clear differentiation of the highest test concentration (96 ng mL^{-1}). A full statistical comparison of cortisol recovery across different extraction times is shown in Fig. S9.

Cortisol recovery within system components showed a strong direct relationship with skin model concentrations for application periods of 15 and 45 min, demonstrating the system's potential for rapid, on-device ISF analysis (Fig. 3c and d). The frequent observation of statistically significant differences between components exposed to different cortisol concentrations further supports the system's ability to discriminate between analyte levels. However, significant differences between distal microfluidic paper segments (MP2 and MP3) and the corresponding skin model concentrations after 15 min suggest that complete analyte equilibration across the channel is not achieved within shorter extraction periods, even when the paper is fully wetted. This effect was reduced after 45 min, with no significant difference observed between MP2 and the skin model. These findings indicate that biosensors and reagents should be positioned closer to the extraction site to improve diagnostic accuracy in short-duration extractions, offering valuable guidance for future system designs.

In contrast, cortisol recovery was reduced for application periods of 24 h, likely due to the instability of cortisol at room temperature and partial fluid evaporation, particularly at more exposed paper microfluidics.[46,47] While skin model biopsies and MNs maintained strong correlation, analyte loss in paper microfluidics suggest susceptibility to environmental degradation at prolonged application periods. This effect is analyte-dependent and should be further investigated with more stable biomarkers. Previous studies have demonstrated continuous extraction, transport, and deposition of analytes in paper microfluidics, indicating that future design improvements may enhance analyte recovery over extended application periods.[41,48–50] Despite reduced accuracy during 24 h extraction periods, the system reliably detected high cortisol concentrations (96 ng mL^{-1}), suggesting semi-quantitative detection remains viable for longer application periods. Integration with biosensors may enable monitoring of analyte degradation and fluid loss during prolonged application, in addition to providing real-time diagnostic results over extended periods.

Lastly, cortisol extraction was evaluated using osmotic pumps loaded with either glycerol or glucose as individual osmogens. Across all system components, only one statistically significantly difference was observed between the osmotic pump configurations (MP2, $p < 0.05$) (Fig. S7). Cortisol concentrations recovered from each component were comparable to those obtained in prior experiments using glycerol alone. Comparative analysis of glycerol and glucose as osmogens driving fluid extraction was also performed to assess how osmogen selection influences analyte recovery. This is particularly relevant for future integration with biosensors, where certain osmogens may interfere with sensing mechanisms or analyte stability. Flexibility in osmogen selection is therefore important for system compatibility across different biomarker targets. Based on the van't Hoff equation (π = iCRT), 12 M glycerol and 4 M glucose generate approximate osmotic pressures of 294 atm and 98 atm, respectively. Despite this threefold difference, negligible variations in extraction efficiency or cortisol recovery were observed, due to the large pressure gradient present in both configurations. These results suggest that once a minimum threshold is surpassed, further increases in osmotic pressure may not yield proportional gains in extraction. However, in human skin, ISF is under a slight negative osmotic pressure (approximately −1 to −4 mmHg),[14] which may necessitate higher osmotic driving forces for effective fluid extraction. These findings indicate that alternative osmogens may be utilized for specific applications (*e.g.*, when necessitated based on analyte compatibility concerns), and further optimization of osmotic driving forces may improve *in vivo* extraction of ISF.

This study was limited to *in vitro* testing using agarose and synthetic skin models, which do not fully encapsulate the mechanical and chemical complexity of human dermis, including vascularization, ISF composition, skin deformation during device application, and surface topology. Additionally,

the MN extraction system was manually assembled on skin models and sectioned for analysis, which may limit reproducibility in real-world applications without further system integration. Furthermore, only a single biomarker was evaluated, and further investigations are necessary to determine the applicability to other clinically relevant analytes in ISF.

System performance in real-world environments may be improved through further development of monolithic device architectures that integrate and prepackage system components together. Additionally, alternative paper microfluidic designs may enable continuous or prolonged fluid extraction. Further integration with biosensors or LFA elements embedded directly within paper microfluidics could enable on-body diagnostics without the need for off-device processing.

Conclusion

This work demonstrates the feasibility of a wearable MN-based platform for minimally invasive ISF extraction and cortisol sampling, using a passive osmotic pumping mechanism integrated with paper microfluidics. The system enabled rapid fluid uptake, consistent lateral transport through paper channels, and quantifiable recovery of cortisol across a physiologically relevant concentration range using skin model surrogates. Notably, strong correlation between skin model concentrations and recovered analyte was observed during short extraction periods, supporting the potential for rapid, on-body point-of-care diagnostics.

Although extended extraction times led to diminished recovery, due to analyte degradation, evaporation, or diffusion limitations—the platform retained sufficient sensitivity to distinguish between elevated cortisol levels, which are clinically meaningful in the context of stress or endocrine disorders. These findings underscore the importance of optimizing sampling duration and integrating stability-enhancing materials for long-term monitoring applications.

Future integration with biosensing modalities may enable real-time, label-free detection and offer new insights into analyte stability, transport kinetics, and temporal dynamics in ISF. Additionally, the platform's passive, zero-power operation, low-cost fabrication, and compatibility with flexible substrates highlight its promise for scalable deployment in wearable health monitoring systems. Overall, this work provides a foundation for the development of next-generation, minimally invasive PoC diagnostics capable of continuous biochemical monitoring outside traditional clinical settings.

Disclosures

This material is based on research sponsored by the Air Force Research Laboratory (AFRL) with SEMI-NBMC under agreement number FA8650-18-2-5402. The U.S. Government is authorized to reproduce and distribute reprints for Governmental purposes notwithstanding any copyright notation thereon. The views and conclusions contained herein are those of the authors and should not be interpreted as necessarily representing the official policies or endorsements, either expressed or implied, of the Air Force Research Laboratory, the U.S. Government, or SEMI. Distribution A. Approved for Public Release: Distribution Unlimited AFRL-2025-3374.

Author contributions

M. D., O. V., and M. D. D. conceived the project. C. S., A. A., I. A., H. N. and J. T. conducted experiments and collected and analysed data. T. S. and S. M. investigated osmotic pumping mechanisms. C. S., A. A., J. T., and M. D. wrote and revised the paper.

Conflicts of interest

M. D. is an officer and founder of DermiSense, Inc. (Cary, NC), which commercializes microneedle-based technologies. The other authors declare no conflicts of interest.

Data availability

Supplementary information is available: The SI document includes a detailed description of methods for flow rate calculations, cortisol quantification in sample matrices, and fluid collection measurements; synthesis and fabrication of methacrylated hyaluronic acid and microneedles; expanded schematics and images of the extraction system and auxiliary components; force measurement data; comparative analysis of glucose and glycerol as osmogens; and additional cortisol extraction results with additional statistical analyses. See DOI: **https://doi.org/10.1039/D5LC00590F**

All data associated with this study are present in the paper or the SI. Raw data that support the findings of this study are available from the corresponding author, M. D., upon reasonable request.

Acknowledgements

This work was supported by National Science Foundation's Center for Advanced Self-Powered Systems of Sensors and Technologies (EEC1160483), NC State Institute for Connected Sensor-Systems and the Chancellor's Innovation Fund, and SEMI-NBMC (NB18-21-26 and NB18-24-38). We acknowledge the assistance in sample preparation from Hanh Tran, Blake Cregg-Wedmore, Akshay Balasubramanian, and Samuel Hoy.

References

1 A. J. Bandodkar, W. J. Jeang, R. Ghaffari and J. A. Rogers, *Annu. Rev. Anal. Chem.*, 2019, **12**, 1–22.

2 L. J. Currano, F. C. Sage, M. Hagedon, L. Hamilton, J. Patrone and K. Gerasopoulos, *Sci. Rep.*, 2018, **8**, 15890.
3 Y. Yang, Y. Song, X. Bo, J. Min, O. S. Pak, L. Zhu, M. Wang, J. Tu, A. Kogan, H. Zhang, T. K. Hsiai, Z. Li and W. Gao, *Nat. Biotechnol.*, 2020, **38**, 217–224.
4 W. Jia, A. J. Bandodkar, G. Valdés-Ramírez, J. R. Windmiller, Z. Yang, J. Ramírez, G. Chan and J. Wang, *Anal. Chem.*, 2013, **85**, 6553–6560.
5 A. Koh, D. Kang, Y. Xue, S. Lee, R. M. Pielak, J. Kim, T. Hwang, S. Min, A. Banks, P. Bastien, M. C. Manco, L. Wang, K. R. Ammann, K.-I. Jang, P. Won, S. Han, R. Ghaffari, U. Paik, M. J. Slepian, G. Balooch, Y. Huang and J. A. Rogers, *Sci. Transl. Med.*, 2016, **8**, 366ra165, DOI: **10.1126/scitranslmed.aaf2593**.
6 T. R. Ray, M. Ivanovic, P. M. Curtis, D. Franklin, K. Guventurk, W. J. Jeang, J. Chafetz, H. Gaertner, G. Young, S. Rebollo, J. B. Model, S. P. Lee, J. Ciraldo, J. T. Reeder, A. Hourlier-Fargette, A. J. Bandodkar, J. Choi, A. J. Aranyosi, R. Ghaffari, S. A. McColley, S. Haymond and J. A. Rogers, *Sci. Transl. Med.*, 2021, **13**, eabd8109, DOI: **10.1126/scitranslmed.abd8109**.
7 D. S. Yang, R. Ghaffari and J. A. Rogers, *Science*, 2023, **379**, 760–761.
8 L. Lyzwinski, M. Elgendi, A. V. Shokurov, T. J. Cuthbert, C. Ahmadizadeh and C. Menon, *Commun. Eng.*, 2023, **2**, 48.
9 Z. Sonner, E. Wilder, J. Heikenfeld, G. Kasting, F. Beyette, D. Swaile, F. Sherman, J. Joyce, J. Hagen, N. Kelley-Loughnane and R. Naik, *Biomicrofluidics*, 2015, **9**, 031301.
10 T. D. La Count, A. Jajack, J. Heikenfeld and G. B. Kasting, *J. Pharm. Sci.*, 2019, **108**, 364–371.
11 P. R. Miller, R. M. Taylor, B. Q. Tran, G. Boyd, T. Glaros, V. H. Chavez, R. Krishnakumar, A. Sinha, K. Poorey, K. P. Williams, S. S. Branda, J. T. Baca and R. Polsky, *Commun. Biol.*, 2018, **1**, 173.
12 R. M. Taylor, P. R. Miller, P. Ebrahimi, R. Polsky and J. T. Baca, *Lab. Anim.*, 2018, **52**, 526–530.
13 B. Q. Tran, P. R. Miller, R. M. Taylor, G. Boyd, P. M. Mach, C. N. Rosenzweig, J. T. Baca, R. Polsky and T. Glaros, *J. Proteome Res.*, 2018, **17**, 479–485.
14 M. Friedel, I. A. P. Thompson, G. Kasting, R. Polsky, D. Cunningham, H. T. Soh and J. Heikenfeld, *Nat. Biomed. Eng.*, 2023, **7**, 1541–1555.
15 K. Aukland and G. Nicolaysen, *Physiol. Rev.*, 1981, **61**, 556–643.
16 P. A. J. Kolarsick, M. A. Kolarsick and C. Goodwin, *J. Dermatol. Nurses' Assoc.*, 2011, **3**, 203–213.
17 A. K. Nilsson, U. Sjöbom, K. Christenson and A. Hellström, *Lipids Health Dis.*, 2019, **18**, 164.
18 K. Y. Baumann, M. K. Church, G. F. Clough, S. R. Quist, M. Schmelz, P. S. Skov, C. D. Anderson, L. K. Tannert, A. M. Giménez-Arnau, S. Frischbutter, J. Scheffel and M. Maurer, *Clin. Transl. Allergy*, 2019, **9**, 24.
19 M. Bodenlenz, K. I. Tiffner, R. Raml, T. Augustin, C. Dragatin, T. Birngruber, D. Schimek, G. Schwagerle, T. R. Pieber, S. G. Raney, I. Kanfer and F. Sinner, *Clin. Pharmacokinet.*, 2017, **56**, 91–98.
20 M. Schiavon, C. Dalla Man, S. Dube, M. Slama, Y. C. Kudva, T. Peyser, A. Basu, R. Basu and C. Cobelli, *Diabetes Technol. Ther.*, 2015, **17**, 825–831.
21 A. Basu, S. Dube, M. Slama, I. Errazuriz, J. C. Amezcua, Y. C. Kudva, T. Peyser, R. E. Carter, C. Cobelli and R. Basu, *Diabetes*, 2013, **62**, 4083–4087.
22 M. G. Allen, M. R. Prausnitz, D. V. McAllister and F. P. M. Cros, Microneedle devices and methods of manufacture and use thereof, *US Pat.*, US6334856B1, 2002.18.
23 P. P. Samant and M. R. Prausnitz, *Proc. Natl. Acad. Sci. U. S. A.*, 2018, **115**, 4583–4588.
24 P. P. Samant, M. M. Niedzwiecki, N. Raviele, V. Tran, J. Mena-Lapaix, D. I. Walker, E. I. Felner, D. P. Jones, G. W. Miller and M. R. Prausnitz, *Sci. Transl. Med.*, 2020, **12**, eaaw0285.
25 H. Takahashi, Y. Jung Heo, N. Arakawa, T. Kan, K. Matsumoto, R. Kawano and I. Shimoyama, *Microsyst. Nanoeng.*, 2016, **2**, 16049.
26 W. Yuan, S. Yang, Yan Feng, L. Zhang, N. Chen and T. Jin, *IJN*, 2012, 1415.
27 M. Rajabi, N. Roxhed, R. Z. Shafagh, T. Haraldson, A. C. Fischer, W. V. D. Wijngaart, G. Stemme and F. Niklaus, *PLoS One*, 2016, **11**, e0166330.
28 H. Xue, J. Jin, X. Huang, Z. Tan, Y. Zeng, G. Lu, X. Hu, K. Chen, Y. Su, X. Hu, X. Peng, L. Jiang and J. Wu, *Nat. Commun.*, 2025, **16**, 2650.
29 Z. Faraji Rad, P. D. Prewett and G. J. Davies, *Beilstein J. Nanotechnol.*, 2021, **12**, 1034–1046.
30 R. K. Mishra, A. M. Vinu Mohan, F. Soto, R. Chrostowski and J. Wang, *Analyst*, 2017, **142**, 918–924.
31 A. Caliò, P. Dardano, V. Di Palma, M. F. Bevilacqua, A. Di Matteo, H. Iuele and L. De Stefano, *Sens. Actuators, B*, 2016, **236**, 343–349.
32 J. Gao, W. Huang, Z. Chen, C. Yi and L. Jiang, *Sens. Actuators, B*, 2019, **287**, 102–110.
33 S. Sharma, A. El-Laboudi, M. Reddy, N. Jugnee, S. Sivasubramaniyam, M. El Sharkawy, P. Georgiou, D. Johnston, N. Oliver and A. E. G. Cass, *Anal. Methods*, 2018, **10**, 2088–2095.
34 A. F. Aroche, H. E. Nissan and M. A. Daniele, *Adv. Healthcare Mater.*, 2025, **14**, 2401782.
35 X. Jiang and P. B. Lillehoj, *Microsyst. Nanoeng.*, 2020, **6**, 96.
36 K. Takeuchi, N. Takama, K. Sharma, O. Paul, P. Ruther, T. Suga and B. Kim, *Drug Delivery Transl. Res.*, 2022, **12**, 435–443.
37 E. C. Wilkirson, D. Li and P. B. Lillehoj, *ACS Sens.*, 2024, **9**, 5792–5801.
38 M. Kadmiel and J. A. Cidlowski, *Trends Pharmacol. Sci.*, 2013, **34**, 518–530.
39 A. J. Vander, J. H. Sherman and D. S. Luciano, *Human physiology: the mechanisms of body function*, McGraw-Hill, Boston, 8th edn, 2001.

40 H. Chang, M. Zheng, X. Yu, A. Than, R. Z. Seeni, R. Kang, J. Tian, D. P. Khanh, L. Liu, P. Chen and C. Xu, *Adv. Mater.*, 2017, **29**, 1702243.
41 T. Saha, T. Songkakul, C. T. Knisely, M. A. Yokus, M. A. Daniele, M. D. Dickey, A. Bozkurt and O. D. Velev, *ACS Sens.*, 2022, **7**, 2037–2048.
42 T. Saha, J. Fang, S. Mukherjee, M. D. Dickey and O. D. Velev, *ACS Appl. Mater. Interfaces*, 2021, **13**, 8071–8081.
43 M. Venugopal, S. K. Arya, G. Chornokur and S. Bhansali, *Sens. Actuators, A*, 2011, **172**, 154–160.
44 S. W. T. Chew, A. H. Shah, M. Zheng, H. Chang, C. Wiraja, T. W. J. Steele and C. Xu, *Bioeng. Transl. Med.*, 2020, **5**, e10157.
45 H. Chang, M. Zheng, X. Yu, A. Than, R. Z. Seeni, R. Kang, J. Tian, D. P. Khanh, L. Liu, P. Chen and C. Xu, *Adv. Mater.*, 2017, 28714117.
46 A. H. Garde and Å. M. Hansen, *Scand. J. Clin. Lab. Invest.*, 2005, **65**, 433–436.
47 P. N. Olson, R. A. Bowen, P. W. Husted and T. M. Nett, *Am. J. Vet. Res.*, 1981, **42**, 1618–1620.
48 E. Elizalde, R. Urteaga and C. L. A. Berli, *Lab Chip*, 2015, **15**, 2173–2180.
49 T. Shay, T. Saha, M. D. Dickey and O. D. Velev, *Biomicrofluidics*, 2020, **14**, 034112.
50 M. M. Gong and D. Sinton, *Chem. Rev.*, 2017, **117**, 8447–8480.